machines

MDPI

Article

Acoustoelastic Theory and Mode Analysis of Bolted Structures Under Preload

Lei Zhao, Rui Kuang, Guizhong Tian *, Xiaona Shi and Li Sun

College of Mechanical Engineering, Jiangsu University of Science and Technology, Zhenjiang 212100, China; zlsxn@foxmail.com (L.Z.); ruik@stu.just.edu.cn (R.K.); shixn@just.edu.cn (X.S.); sunl@just.edu.cn (L.S.)
* Correspondence: zhaogoe@just.edu.cn

Abstract: Bolted connections are a common feature of connection in mechanical structures, employed to secure connected parts by tightening nuts and providing preload. The preload is susceptible to various factors leading to potential bolt loosening. The acoustoelastic theory is the most common measure of a bolt structure's stress. The present study investigates the relationship between the inherent properties of a structure and its acousticelastic properties. The modal response of the bolted structure under different preload forces is studied by translating the acoustoelastic relationship of the structure into an analysis of its intrinsic properties. The modal analysis reflects the relative change in wave velocity to be determined implicitly based on the eigenfrequencies of the structure. A frequency formulation of classical bolted structures based on acoustoelastic theory is presented in this paper to conduct the intrinsic characteristic analysis of bolted structures. The COMSOL5.4 simulation results are under the acoustic elasticity coefficients for ultrasonic wave propagation in bolt structures, as predicted by the acoustic elasticity theory, and the present solutions are compared with those available in the literature to confirm their validity. A systematic parameter study for bolted structures under the varying preloads with different material parameters, Lame elastic constants, Murnaghan third-order elastic constants, and structural parameters are presented. These results may serve as a benchmark for researchers in this field.

Keywords: bolt structure; preload; acoustoelastic theory; fundamental frequency

Citation: Zhao, L.; Kuang, R.; Tian, G.; Shi, X.; Sun, L. Acoustoelastic Theory and Mode Analysis of Bolted Structures Under Preload. *Machines* **2024**, *12*, 822. https://doi.org/10.3390/machines12110822

Academic Editor: Ciro Santus

Received: 17 October 2024
Revised: 8 November 2024
Accepted: 15 November 2024
Published: 18 November 2024

1. Introduction

Threaded connections are a common and versatile option in engineering structural and mechanical design, applied in various equipment and components, including wind turbines, drilling rigs, bridges, and engines. It is crucial to ensure the stability and safety of threaded connections by providing a sufficient preload. An insufficient preload may result in relative movement between the connected parts. In contrast, an excessive preload may lead to the failure of the threaded connection strength or local damage to the mechanical structure. Both possibilities are damaging to the structural stability of engineering structures. It is, consequently, vital that bolt preload is checked and recorded regularly in order to ensure the safe operation of mechanical equipment.

There are numerous methodologies for testing bolt preload. The torque control method calculates the preload force by measuring the torque applied to the bolt and is widely used in mechanical assembly [1]. The optical mechanics method is widely used in high-precision testing by using optical technology to monitor the tiny deformation of bolts to calculate the preload [2]. The resistance strain gauge detects the axial stress of the bolt by sensing the surface strain of the bolt, providing a high degree of accuracy in the measurement of bolt stress [3]. By measuring the magnetic field change caused by the bolt force, the magnetoresistive sensor calculates that the preload force has a high anti-overload capability and can work under harsh environmental conditions [4]. However, the torque control method is affected by the change in the friction coefficient, which may lead to a

detection error; the photomechanical method is limited by equipment cost, environmental interference and installation requirements and other factors; excessive stress applied by the resistance strain gauge may exceed the linear range, resulting in lower measurement accuracy; and magnetoresistive sensors are limited by magnetic field interference and depend heavily on material characteristics. The ultrasonic method is a widely used method to detect the axial stress of bolts. The basic premise of the ultrasonic method is based on the idea of acoustic elasticity, that is, the speed of ultrasonic propagation changes with the change of stress. The axial tension of the bolt can be determined indirectly by measuring the time the ultrasonic pulse passes through the bolt.

A substantial body of research has been conducted by both domestic and international scholars on the methodology for measuring axial stress in bolts using the theory of ultrasonic acoustoelastic. The detection of ultrasonic stress represents a fundamental aspect of non-destructive testing, given the capacity of ultrasonic waves to penetrate deeply and rapidly propagate through the material under examination. This quality endows the technique with significant versatility, rendering it suitable for a wide range of testing scenarios. In a study by Yan Lv et al. [5,6], based on the principle of acoustoelastic effect, the axial stress of bolts was measured by a longitudinal and transverse wave combination method and signal inter-correlation algorithm. Shan Gao et al. [7] optimized an electromagnetic ultrasonic transducer by analyzing the propagation characteristics of ultrasonic waveforms and application scenarios and modelled the multi-physics field coupling in COMSOL. Sang-Hyung Lee et al. [8] proposed an ultrasonic detection method of the pre-tension force of high strength bolts based on the principle of the double wave method, which is easy to operate and has high accuracy, and can effectively improve the accuracy of detecting the pre-tension force of bolts. Qinxue Pan et al. [9] showed, by normalization and polynomial fitting, that a functional relationship between bolt axial stress and normalized relative nonlinear coefficients can be established to achieve high accuracy bolt axial stress detection. Sheng Feng et al. [10,11] studied the bolt stress ultrasonic inspection process and procedure by establishing an acoustic elasticity coefficient calculation model, analyzing the temperature effect and optimizing the inspection process. S. OKA [12] discovered the acoustoelastic phenomenon in elastic materials, namely, the correlation between sound wave propagation speed and stress, making it possible to measure structural stress through changes in sound velocity indirectly. Janusz et al. [13] created a piezoelectric self-excited acoustic device to monitor structural stress variations. A mathematical model combining various factors, including the acousticelastic coefficient and ultrasonic acoustic time, was constructed and later verified using finite element simulation and testing. Xin-Xin Zhao et al. [14] measured the axial force of high-strength bolts in railway steel bridges by accurately distinguishing the different force regions of the bolts and calculating the ultrasonic propagation time in each region. Moradi et al. [15] proved experimentally that bolt axial stresses have a significant effect on the change in ultrasonic sound velocity, and the presence of shear stresses leads to a further decrease in the ultrasonic sound velocity. Brandon Mills et al. [16] validated the PAUT as a powerful tool for enhancing the safety and longevity of wind turbine towers for bolts of different sizes, materials, and tightening depths.

The relationship between the natural frequency of a structure and bolt preload remains an area of ongoing research, and this paper addresses this topic as its primary focus. Mode analysis is a method used to analyze a structure's natural frequency and mode. It is one of the most commonly employed techniques for quantifying the dynamic behavior of a structure in vibration analysis. Mode analysis can be employed to corroborate the precision of finite element models, assess the dynamic attributes of structures, identify vulnerable points within structures, regulate system noise, modify the system dynamic parameters, determine the optimal part installation positions, and ascertain the system health status.

By analyzing the structure's natural frequency characteristics, the structural stiffness change can be identified, and the location and degree of damage can be determined [17]. In accordance with the principles of vibration theory, any given structure can be regarded as a system comprising a number of physical properties, including stiffness and mass. Any

alteration to these physical properties will affect the structure's dynamic parameters, such as its mode natural frequency. Consequently, the measurement of alterations in these dynamic parameters enables the inference of the structural damage state. Prior research has indicated that the stiffness of bolt joint surfaces is subject to variation in response to alterations in bolt preload [18]. Gou Baiyong et al. [19] employed the Mahalanobis square distance outlier analysis method to quantitatively assess bolt pretension force by applying the first five-order natural frequencies of bending modes to the structure. An analysis of the first six natural frequencies of the structure was conducted by Weiwei et al. [20], which allowed them to determine the function curve between spring stiffness and natural frequency. This resulted in an accuracy error of less than 8% in identifying stiffness. Zhao Gong et al. [21] employed the hammer mode test method to determine the parameters of the virtual material and to analyze the influence of bolt preload on mode frequency. The test results indicated that when the bolt tension increased, there was a distinct trend for the natural frequencies to climb in accordance with each order. Zhao et al. [22] determined the bolted connection stiffness in reverse by an examination of the first six-order mode natural frequencies. The findings demonstrated that an increase in stress resulted in an overall rise in natural frequency, which the comparable joint stiffness of the virtual material can adequately reflect. Sah et al. [23] conducted a transverse impact experiment to create bolt-bending vibration in two bolt heads of various lengths. The relationship between the transverse first natural frequency and the bolt pretension force was established to assess the bolts' tightness. Bonisoli et al. [24] investigated the influence of the stress-hardening effect induced by interference fit on the structural modal properties and provided a basis for the dynamic analysis of interference fit design. Faria and Donadon [25] explored the use of the stress-hardening effect of piezoelectric materials to enhance the flexural properties of laminates and verified the effectiveness of piezoelectric prestressing in improving structural stability.

This study explores the impact of bolt preload on the inherent frequency, with a particular emphasis on the detection of bolt tension through the acoustoelastic effect of ultrasound. Furthermore, the influence of stress on the intrinsic frequency characteristics is investigated through mode analysis. Firstly, this paper presents an overview of the most widely used methods for bolt detection and the current status of research in ultrasonic acoustoelastic detection and mode analysis. Secondly, it gives the calculation equation for bolt strain and the acoustoelastic theory, utilizing the structure's natural frequency to evaluate axial forces through mode analysis. Thirdly, mode analysis of a bolted structure is undertaken using simulation software to explore the change in frequency under different preload settings and assess the influence of various parameters on the stress state. The final section gives a summary, and conclusions based on the paper are drawn accordingly.

2. Analytic Theory

2.1. The Preload of Bolted Structure

In most instances, the bolted structure must be adequately fastened during the installation process to guarantee that it is adequately preloaded prior to bearing the anticipated working load. The application of preload force enhances the tightness and reliability of the connection and prevents the formation of gaps or relative sliding after loading [26,27].

When utilizing a torque wrench to regulate preload, the tightening torque of the bolt can be calculated by adding together the friction torque exerted between the nut end face and the connected component's supporting surface and the friction torque between the bolt and the nut thread. In this instance, ϕ denotes the tooth side angle, while φ_v indicates the equivalent friction angle. Figure 1 demonstrates the force analysis of the thread, illustrating a transverse force acting on the thread surface.

$$F' = Ftan(\phi + \varphi_v) \quad (1)$$

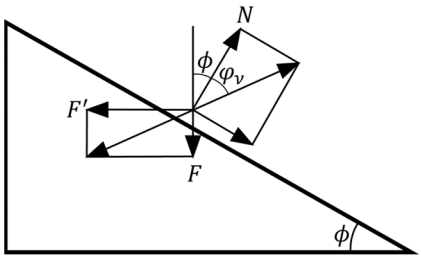

Figure 1. Force analysis of thread.

Therefore, the friction torque between the bolt thread and the nut thread can be expressed as follows:

$$M_1 = F'\frac{d_2}{2} = F\frac{d_2}{2}\tan(\phi + \varphi_v) \tag{2}$$

According to the basic calculation equation of friction force (3), Equation (4) give the area between the nut end face and the supporting surface of the connected piece:

$$f_c = uF \tag{3}$$

$$A = \pi\left[\left(\frac{D_0}{2}\right)^2 - \left(\frac{d_0}{2}\right)^2\right] = \frac{\pi}{4}\left(D_0^2 - d_0^2\right) \tag{4}$$

According to this, the friction force per unit area can be determined as follows:

$$\rho_c = \frac{f_c}{A} = \frac{4uF}{\pi\left({D_0}^2 - {d_0}^2\right)} \tag{5}$$

Therefore, the friction torque between the end face of the nut and the supporting surface of the connected part can be expressed as follows:

$$\begin{aligned} M_2 &= \int_{\frac{d_0}{2}}^{\frac{D_0}{2}} \rho_c \cdot r \cdot 2\pi r dr = \int_{\frac{d_0}{2}}^{\frac{D_0}{2}} \frac{4uF}{\pi\left({D_0}^2 - {d_0}^2\right)} \cdot 2\pi r^2 dr \\ &= \frac{8uF}{\left({D_0}^2 - {d_0}^2\right)} \cdot \frac{1}{3}\left[\left(\frac{D_0}{2}\right)^3 - \left(\frac{d_0}{2}\right)^3\right] = \frac{uF\left({D_0}^3 - {d_0}^3\right)}{3\left({D_0}^2 - {d_0}^2\right)} \end{aligned} \tag{6}$$

According to the tightening torque T, the friction torque M_1 between the bolt thread and the nut thread, and the friction torque M_2 between the nut end face and the supporting surface of the connected piece, can be determined as follows:

$$T = M_1 + M_2 = \frac{1}{2}F\left[d_2\tan(\phi + \varphi_v) + \frac{2u}{3}\frac{D_0^3 - d_0^3}{D_0^2 - d_0^2}\right] \tag{7}$$

where, d_0 is the diameter of bolt hole, φ_v is the equivalent friction angle, u is the friction coefficient, and D_0 is the nut outside diameter.

The above parameters are put into Equation (7), and the direct relationship between tightening torque and preloading force can be obtained:

$$T \approx 0.196Fd \tag{8}$$

2.2. Acoustoelastic Theory

The elastic modulus of the solid material undergoes slight alterations in response to stress, and the material's elastic modulus is directly proportional to the propagation velocity

of the ultrasonic wave. It can, thus, be surmised that fluctuations in the internal tension of a solid material will result in variations in the speed of ultrasonic waves. This provides the basis for the acoustic elastic effects-based stress detection of materials. The solid acoustic elastic effect has the potential to be utilized in two principal ways for the measurement of stress in structural components. Firstly, the speed of ultrasonic waves propagating through structural components depends on their internal stress, thereby providing a theoretical basis for stress detection. Secondly, developments in sensing technology and signal acquisition and processing methods facilitate the precise transmission and reception of ultrasonic waves and high-frequency signal sampling. In particular, existing signal analysis techniques can precisely identify ultrasonic propagation sounds at the nanosecond level, thereby providing technical support for the stress detection of structural components.

The results of research conducted thus far indicate that the elastic modulus of a material increases with compressive stress and decreases with tensile stress. This suggests a non-linear relationship between stress and strain in materials. Given that the speed of ultrasonic waves depends on the material's elastic modulus in question, it follows that stress induces changes in the material's elastic modulus, thereby leading to alterations in the ultrasonic wave velocity. The non-linear relationship between the internal stress and the strain of a material can be expressed by the following equation:

$$e = E_0\varepsilon + \frac{1}{2}E_1\varepsilon^2 + \frac{1}{6}E_2\varepsilon^3 + \frac{1}{24}E_3\varepsilon^4 + \dots \tag{9}$$

where E_i is the i-order elastic coefficient of the material, $i = 0 \sim n$, e is the strain energy, and ε is the strain.

It is obtained by the differentiating of Equation (9) as follows:

$$\sigma = \frac{de}{d\varepsilon} = E_0 + E_1\varepsilon + \frac{1}{2}E_2\varepsilon^2 + \frac{1}{6}E_3\varepsilon^3 + \dots \tag{10}$$

where σ is the stress of the material.

It is hypothesized that $E_0 = 0$, and when the higher order term in Equation (10) above is removed, the following is obtained:

$$\sigma = \frac{de}{d\varepsilon} = \left(E_1 + \frac{1}{2}E_2\varepsilon\right)\varepsilon = E'\varepsilon \tag{11}$$

where E' is the effective elastic modulus of the material.

When an elastic wave propagates in a solid, the velocity of the longitudinal wave is related to the elastic modulus and density of the material; it can be written as follows:

$$V_L = \sqrt{\frac{E'}{\rho_0}} \tag{12}$$

where V_L is the longitudinal wave velocity and ρ_0 is the density of the material under no force.

In this way, the connection between the wave velocity and stress can be established through the effective elastic modulus, which varies with the stress within the material. This forms the basis of the correlation between sound velocity and stress.

Based on the solid acoustoelastic theory, the relationship between the wave velocity V and stress σ in the direction of stress in an isotropic solid under simple loading can be derived:

$$\begin{gathered} \rho_0 V_L^2 = \lambda + 2\mu + \frac{\sigma}{3\lambda+2\mu}\left[\frac{\lambda+\mu}{\mu}(4\lambda + 10\mu + 4m) + \lambda + 2l\right] \\ \rho_0 V_T^2 = \mu + \frac{\sigma}{3\lambda+2\mu}\left[\frac{\lambda n}{4\mu} + 4\lambda + 4\mu + m\right] \end{gathered} \tag{13}$$

where V_L is the velocity of the longitudinal wave propagating along the uniaxial stress direction, V_T is the velocity of the transverse wave propagating along the uniaxial stress

direction, λ, μ is the second-order elastic constant of the isotropic medium, namely, the Lame constant, l, m, n is the third-order elastic constant of the isotropic medium, namely, the Murnaghan constant, and σ is the uniaxial stress on the isotropic media.

The propagation velocity of the longitudinal wave in a body without stress (i.e., $\sigma = 0$) can be obtained from Equation (13):

$$V_{L0} = \sqrt{\frac{\lambda + 2\mu}{\rho_0}} \tag{14}$$

It is assumed that the relative change is small; the relative change in the wave velocity with axial strain can be calculated from Equations (13) and (14):

$$dV_L = \frac{\left[\frac{\lambda+\mu}{\mu}(4\lambda + 10\mu + 4m) + \lambda + 2l\right]}{2\rho_0 V_L(3\lambda + 2\mu)} d\sigma \tag{15}$$

$$\frac{dV_L/V_{L0}}{d\sigma} = \frac{\frac{\lambda+\mu}{\mu}(4\lambda + 10\mu + 4m) + \lambda + 2l}{2(\lambda + 2\mu)(3\lambda + 2\mu)} \tag{16}$$

Because the strain is very small, it is assumed that there is a linear relationship between the stress and strain, that is, $\sigma = E \cdot \varepsilon$. From Equation (16), the acoustic elastic coefficient of the longitudinal wave when the dimensionless propagation direction is parallel to the stress direction can be further obtained:

$$L = \frac{dV_L/V_{L0}}{d\varepsilon} = \frac{E\left[\frac{\lambda+\mu}{\mu}(4\lambda + 10\mu + 4m) + \lambda + 2l\right]}{2(\lambda + 2\mu)(3\lambda + 2\mu)} \tag{17}$$

According to the relationship between the Lame constants λ, μ and the elastic constant E ($E = \frac{\mu(3\lambda+2\mu)}{\lambda+\mu}$) of linear elastic materials, the following equation is obtained:

$$L = \frac{dV_L/V_{L0}}{d\varepsilon} = \frac{(\lambda + \mu)(4\lambda + 10\mu + 4m) + \lambda\mu + 2\mu l}{2(\lambda + \mu)(\lambda + 2\mu)} \tag{18}$$

The acoustic elastic coefficient, related to the solid's elastic modulus and the second- and third-order elastic constants, and other pertinent quantities, represents the rate of change in the ultrasonic wave velocity brought on by the strain. However, it is a difficult measurement to obtain since the acoustic elastic coefficient cannot be tested directly using equipment. Therefore, we verified the change regulation of the structure's acoustic elastic coefficient under preload by investigating its inherent properties.

In acoustoelastic simulations and tests, the propagation time is typically measured directly. However, tensile strain occurs when the bolted structure is subjected to preload. Instead of directly computing the wave speed, which can be a difficult task, the structure's eigenfrequencies are used to obtain the wave speed implicitly. The relative change in the wave velocity is defined as $\frac{V_\sigma - V_0}{V_0}$, and the relative change in the wave velocity under unit strain is $\frac{V_\sigma - V_0}{\varepsilon V_0}$.

When the tensile strain is not considered, the relative variability of the wave speed is calculated as follows:

$$K' = \frac{V_\sigma - V_0}{\varepsilon V_0} \tag{19}$$

In the post-tensile measurement, the respective propagation times are calculated as shown in Equations (20) and (21) due to the existence of tensile strain.

$$V_0 = \frac{L}{t_0} = L \cdot f \tag{20}$$

$$V_\sigma = \frac{L + \Delta L}{t_\sigma} = \frac{(1+\varepsilon)L}{t_\sigma} = (1+\varepsilon)\cdot L \cdot f_\sigma \tag{21}$$

Therefore, the equation for calculating the relative variation value of the wave velocity can be expressed as Equation (22):

$$K' = \frac{V_\sigma - V_0}{\varepsilon V_0} = \frac{(1+\varepsilon)Lf_\sigma - Lf}{\varepsilon Lf} = \frac{f_\sigma - f}{\varepsilon f} + \frac{f_\sigma - f}{f} + 1 = \left(\frac{1}{\varepsilon} + 1\right)\frac{f_\sigma}{f} - \frac{1}{\varepsilon} \tag{22}$$

It is evident that the investigation moves beyond the structure's acoustoelastic relationship to look at its underlying properties. Moreover, it offers a more thorough description of how bolt preload and structural natural frequency are related.

3. Results and Discussion

As shown in Figure 2, the test structure consists of two square steel cubes, 100 mm long, 100 mm wide, and 80 mm high, together with a bolt and nut. The bolts are used to fix the center of the specimen, which has a through hole; the diameter and material parameters of which are given in Table 1. The hyperelastic materials are assigned to the bolts and nuts, while the linear elastic materials are assigned to the connectors to capture the acoustoelastic properties of the bolts better.

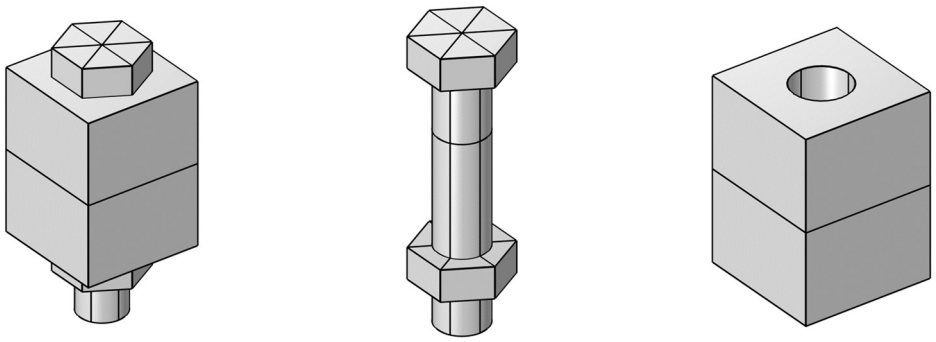

Figure 2. Sample model.

Table 1. Material parameters.

Parameters		Bolts and Nuts	Connected Structures
Density (kg/m^3)	ρ	7850	7850
Young's modulus (GPa)	E	/	205
Poisson's ratio	v	/	0.28
Lame constants (GPa)	λ μ	115.8 79.9	/ /
Murnaghan constants (GPa)	l m n	−248 −623 −714	/ / /

COMSOL was used for simulation, and the boundary conditions were set as follows:

(1) Boundary conditions: Using the solid mechanics physical field, the upper surface of the square steel is set as a fixed constraint, and the bottom end of the screw is set as a specified displacement.
(2) Mesh division: Tetrahedral mesh division is used for the bolt head and nut, and the sweeping division method is used for the bolt rod and square steel.
(3) Post-processing: Steady-state analysis and characteristic frequency analysis are adopted to import the simulation data related to frequency and strain into Origin for data processing and draw the correlation curve.

3.1. Modes Analysis of Preload on Bolted Structure

3.1.1. The Modes of the Bolted Structure Under the Non-Stress Conditions

Prior to conducting a formal study on the service performance of bolted structures, an analysis of the mode characteristics of bolted structures in a non-stress state was performed. The research data for simulating the behavior of bolted structures in service were accumulated by studying the structural modes in an unconstrained state, and an estimation was made regarding the range of characteristic frequencies.

Figure 3 illustrates the three modes of the outer hexagonal bolt in the free boundaries. The bending mode presents a significant challenge in achieving single-mode excitation and recognition, largely due to the complex dispersion characteristics and the prevalence of mode aliasing during practical operation. Due to axial symmetry, the torsional mode exhibits circumferential displacement in the wave structure's displacement distribution, with zero radial and axial displacement components. Its waveform resembles the A-mode and SH wave in a plate, representing a special form of shear wave. The longitudinal mode also has axial symmetry, which makes it less vulnerable to interference from other modes and, therefore, it is simpler to establish single-mode excitation.

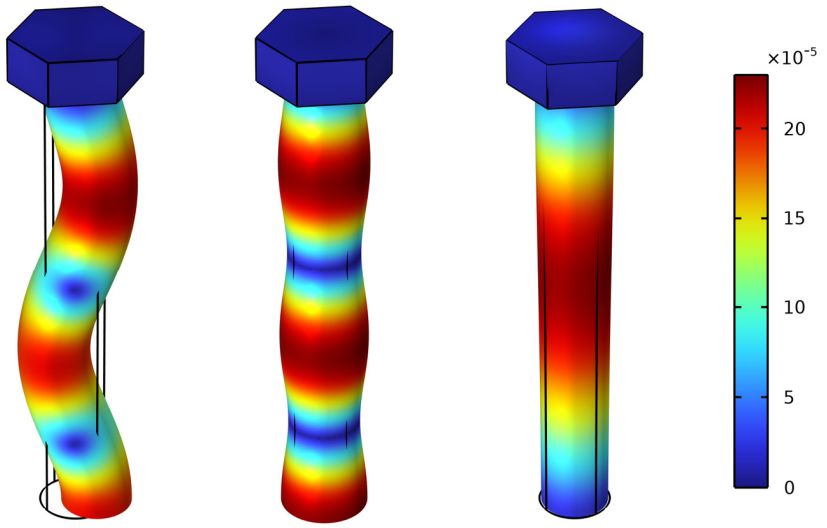

Figure 3. Different mode changes of bolted structure in the non-stress state.

3.1.2. Verification of the Characteristic Frequency and Preload

The application of preload to a bolted connection places the bolt in a tensile condition, thereby ensuring that the bolt and the connecting member come into direct contact with one another. The components are firmly fixed together by the preloading force, which also provides them with the necessary tolerance for loads and external forces. In order to ensure reliability and security, it is essential that the preload force is properly determined and applied in accordance with the operating circumstances and specifications of the associated parts. In practical engineering, the ability to adjust and control bolted connections' preload is paramount for maintaining stability and reliability.

Upon substituting Lame elastic constants and Murnaghan's third-order elastic constants from Table 1 into Equation (18) [28], an acoustic elasticity coefficient value of L of -2.5 is obtained. To illustrate, the eigenfrequencies of an M30 $\times$ 200 mm hexagonal bolt in both its free state and at a strain of 0.001 are calculated in COMSOL Multiphysics. Figure 4a represents the bending-torsion longitudinal modal diagram of the bolt in its free condition. In contrast, Figure 4b illustrates the bending-torsion longitudinal modal pattern of the bolt when exposed to tensile strain. When a bolt is subjected to tensile strain, both its length and its prestressed state change, resulting in a shift in the wave velocity within the

material. Taking its longitudinal mode as an example, the frequency in the free state is 12,414 Hz. According to Equation (20), when the bolt length is fixed, the sound velocity is only related to the frequency. When subjected to a stress that generates 0.001 strain, its frequency is 12,366 Hz. It can be seen from Equation (21) that the sound velocity is related to the frequency and strain when the bolt length is fixed. Substituting the value of the frequency in the free state and the value of the frequency in the strain state into Equation (22) provides a value of −2.8, which matches well with the value determined using Equation (18).

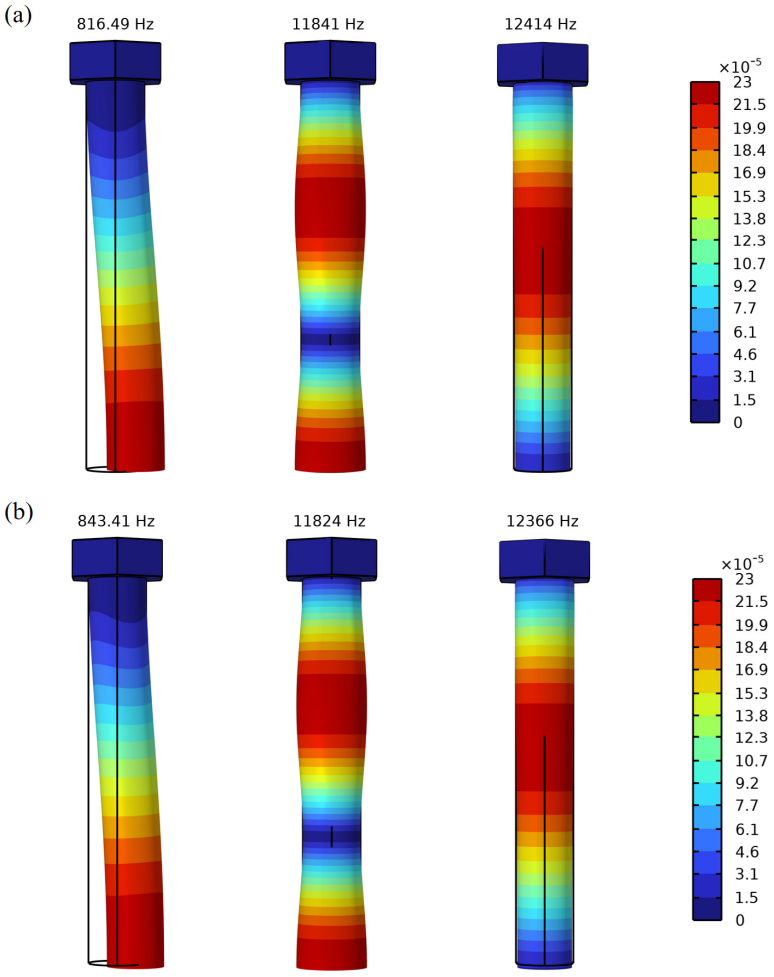

Figure 4. The different modes of bolts under various strains. (**a**) different modes of bolts without strain; (**b**) different modes of bolts under 0.001 strain.

Figure 4 illustrates that the eigenfrequencies of the bolted structure exhibit variability when the structure is in different states. This allows for the establishment of a relationship between wave speed and stress based on the relative change in wave speed. Consequently, the assessment of pre-stressing can be conducted by examining the shift in the eigenfrequency of the workpiece.

3.2. Influence of Material and Structural Parameters

3.2.1. Influence of Bolt Material Parameters on Natural Frequency Characteristics

The contact state of the bolted joint structure is contingent upon factors such as the material and the actual load, which significantly influence the structure's dynamic properties. Therefore, it is imperative to investigate the impact of varying material factors on the intrinsic properties of the bolted structure. Table 2 presents the material parameters of the bolted structure.

Table 2. Material parameters.

Materials	λ (GPa)	μ (GPa)	l (GPa)	m (GPa)	n (GPa)
high manganese steel	115.8	79.9	−248	−623	−714
45 steel	111.59	81.79	−81.25	−583.1	−782.85
nickel steel	109	81.7	−56	−671	−785
high-strength steel	109	82	−426	−619	−708
20 steel	116.8	80.6	−69	−574	−670

Figure 5 depicts the impact of varied preloading pressures on the fundamental frequency variation across distinct modes. It may be proved that the fundamental frequencies of bolted constructions display analogous tendencies across different modes. Nevertheless, it is obvious that different materials exert varying degrees of effect on the modes. In the case of bending modes, an increase in strain is accompanied by an increase in frequency, whereas in the case of torsional modes, an increase in strain is accompanied by a decrease in frequency. Similarly, the change in the longitudinal mode follows a pattern comparable to that of the torsional mode, exhibiting a decline with increasing strain. However, there is a disparity of roughly 155 Hz between different materials in the torsional mode frequency range, with a reasonably dense distribution interval of around 105 Hz, compared to the longitudinal mode. It is noticed that the material parameters exert the least influence on the bending mode, followed by the longitudinal mode. Conversely, the torsional mode is the most strongly influenced. The frequency range for all three modes stays relatively small when the strain is less than 10^{-4}. However, considerable variations in frequency values are detected as the strain increases from 10^{-4} to 10^{-2}, with the bending mode frequency exhibiting a notable increase while both the torsional and longitudinal modes experience a pronounced decrease.

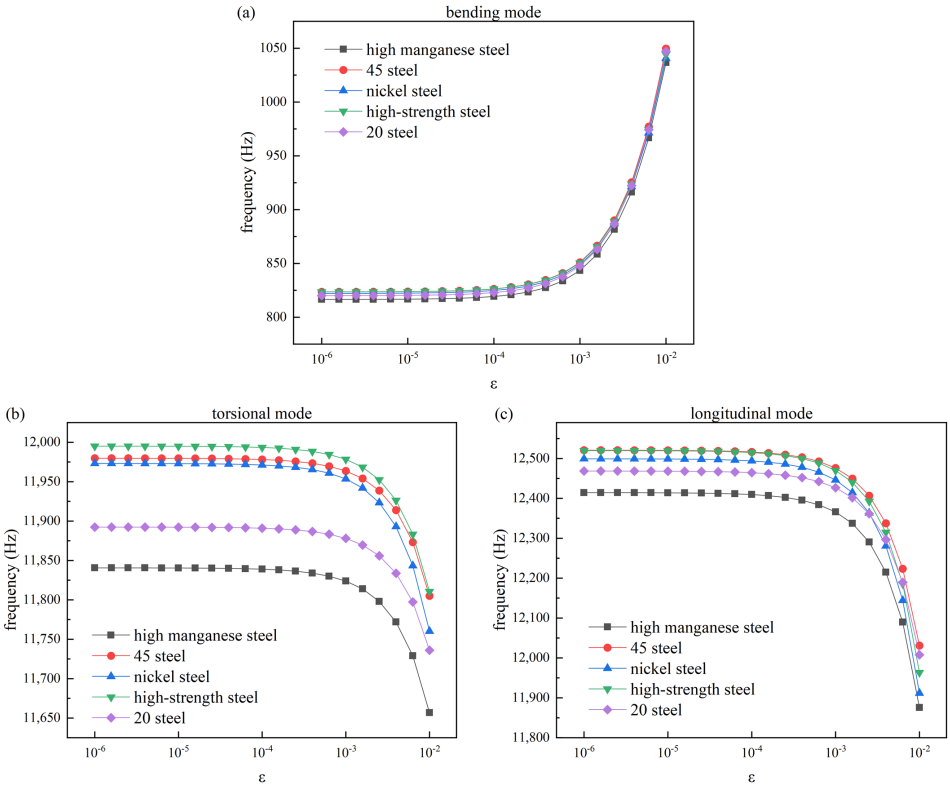

Figure 5. Changes in frequencies with different modes under the strain of five different materials. (**a**) changes in frequencies with bending modes under the strain of five different materials; (**b**) changes in frequencies with torsional modes under the strain of five different materials; (**c**) changes in frequencies with longitudinalmodes under the strain of five different materials.

Figure 5 illustrates that the fundamental frequencies of bolted structures comprising different materials exhibit comparable variation patterns. Therefore, the effect of the material parameters, namely, Lame second-order elastic constants λ, μ and Murnaghan third-order elastic constants l, m, n, on the fundamental frequencies of bolts under varying strains will be the primary focus of the analysis. The following analysis will be conducted using high manganese steel as the base material for bolts.

Figure 6 illustrates the correlation between the Lame elastic constant and strain on the fundamental frequency of the structure. Figure 6a depicts the Lame elastic constant λ, whereas Figure 6b illustrates the Lame elastic constant μ. The numbers 1, 2, and 3 correspond to the bending mode, torsional mode, and longitudinal mode, respectively.

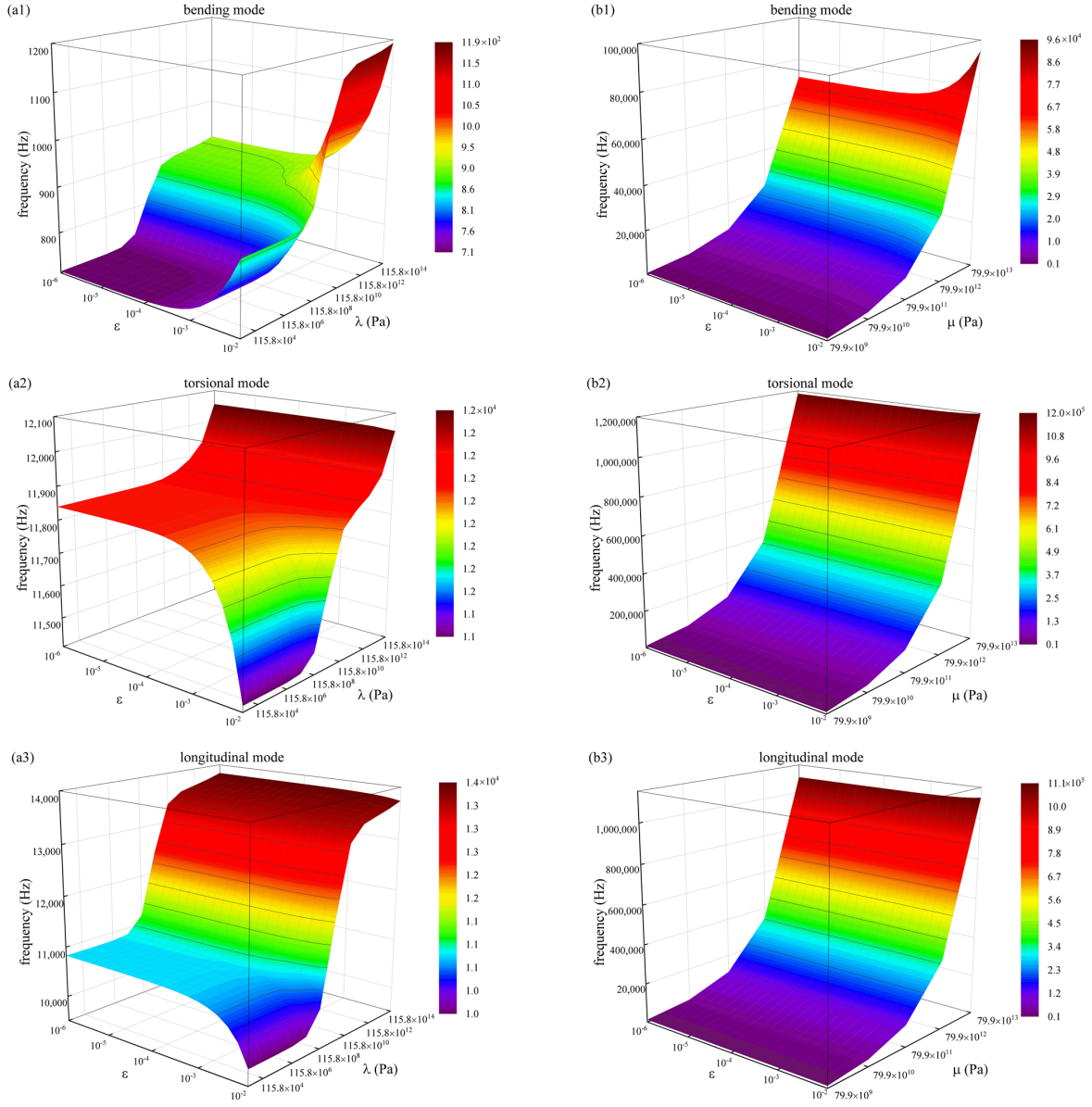

Figure 6. Surface diagram of mode frequency under strain and elastic constant of Lame. (**a1**) surface diagram of bending mode frequency under strain and λ; (**a2**) surface diagram of torsional mode frequency under strain and λ; (**a3**) surface diagram of longitudinal mode frequency under strain and λ; (**b1**) surface diagram of bending mode frequency under strain and μ; (**b2**) surface diagram of torsional mode frequency under strain and μ; (**b3**) surface diagram of longitudinal mode frequency under strain and μ.

As shown in Figure 6a, the frequency of the bolt structure will change when the strain and the Lame elastic constant λ are different. As illustrated in Figure 6(a1), there is a gradual transition in frequency when the strain $\varepsilon \in [0,10^{-4}]$ and $\lambda \in [115.8\times10^{3}, 115.8\times10^{7}]$ Pa for the bending mode. However, when the strain $\varepsilon \in [10^{-4}, 10^{-2}]$ and $\lambda \in [115.8\times10^{3}, 115.8\times10^{7}]$ Pa, there is an increase in frequency with increasing strain. Similarly, an increase in frequency is observed with an increase in parameter λ when the strain $\varepsilon \in [0,10^{-2}]$ and $\lambda \in [115.8\times10^{7}, 115.8\times10^{10}]$ Pa. In the case where the strain $\varepsilon \in [0,10^{-4}]$ and $\lambda \in [115.8\times10^{10}, 115.8\times10^{14}]$ Pa there is a slight increase in frequency as λ increases. Conversely, there is a notable increase in frequency when the strain $\varepsilon \in [10^{-4}, 10^{-2}]$ and $\lambda \in [115.8\times10^{10}, 115.8\times10^{14}]$ Pa. This is evident in the torsional mode illustrated in Figure 6(a2). In the case where $\lambda \in [115.8\times10^{3}, 115.8\times10^{10}]$ Pa and $\varepsilon \in [0,10^{-4}]$, the variation of frequency is relatively minor. However, when $\varepsilon \in [10^{-4}, 10^{-2}]$, there is a notable decrease in frequency with the increase of the strain. When the strain $\varepsilon \in [0,10^{-2}]$ and $\lambda \in [115.8\times10^{10}, 115.8\times10^{14}]$ Pa, there is an increase in frequency with an increase in λ. With regard to the longitudinal mode illustrated in Figure 6(a3), it can be observed that when $\lambda \in [115.8\times10^{3}, 115.8\times10^{7}]$ Pa and $\varepsilon \in [0,10^{-4}]$, there is minimal variation in frequency. Conversely, when $\varepsilon \in [10^{-4}, 10^{-2}]$ and $\lambda \in [115.8\times10^{3}, 115.8\times10^{7}]$ Pa, there is a notable decline in frequency as the strain increases. However, when the strain $\varepsilon \in [0,10^{-2}]$ and the wavelength $\lambda \in [115.8\times10^{7}, 115.8\times10^{10}]$ Pa, the frequency increases significantly with an increase in λ. In contrast, when $\lambda \in [115.8\times10^{10}, 115.8\times10^{14}]$ Pa, the frequency increases gradually with an increase in λ.

Figure 6b depicts the correlation between the frequency of the bolted structure and alterations in strain and the Lame elastic constant μ. In the bending mode, torsional mode, and longitudinal mode, a uniform overall tendency is observed, characterized by a notable rise in frequency. However, in the bending mode, there is minimal variation in frequency with strain for changes in strain when μ is within the range of 79.9×10^{9} to 79.9×10^{12} Pa. It is only when μ reaches 79.9×10^{13} Pa that a notable increase in frequency is observed with an increase in strain. In the torsional and longitudinal modes, a slight increase in frequency is evident as strain increases.

As illustrated in Figure 7, the correlations between Murnaghan's third-order elastic constants and strain on the fundamental frequency of the structure are presented. Figure 7a illustrates the relationship between the frequency of the bolted structure and the Murnaghan third-order elastic constant l, as well as the effect of strain on this frequency. For the bending mode shown in Figure 7(a1), an increase in strain leads to a significant increase in frequency, while an increase in l results in a minimal change in frequency. With regard to the torsional mode depicted in Figure 7(a2) and the longitudinal mode shown in Figure 7(a3), an increase in strain results in a notable decrease in frequency, whereas variations in l give rise to a smaller range of frequency change.

Figure 7b illustrates that the frequency of the bolted structure changes in response to alterations in the strain and the third-order elastic constant m of the Murnaghan model. With regard to the bending mode (Figure 7(b1)), it is evident that the frequency increases markedly in conjunction with an increase in the strain. When the strain is less than 10^{-2}, the frequency undergoes a gradual change with an increase in m. At a strain of 10^{-2}, the frequency exhibits a significant increase in $m \in [-623\times10^{9}, -623\times10^{8}]$Pa, followed by a less pronounced change.

For the torsional mode Figure 7(b2) and the longitudinal mode Figure 7(b3), the degree to which the frequency changes with strain and m is similar overall. When the strain $\varepsilon \in [0, 10^{-4}]$ and $m \in [-623\times10^{9}, -623\times10^{3}]$ Pa, the frequency hardly changes. When $\varepsilon \in [10^{-4}, 10^{-2}]$ and $m \in [-623\times10^{7}, -623\times10^{3}]$ Pa, the frequency increases with the increase of strain, and almost does not change with the increase of m. When $\varepsilon \in [10^{-4}, 10^{-2}]$ and $m \in [-623\times10^{9}, -623\times10^{7}]$ Pa, the frequency increases sharply with the increase in strain.

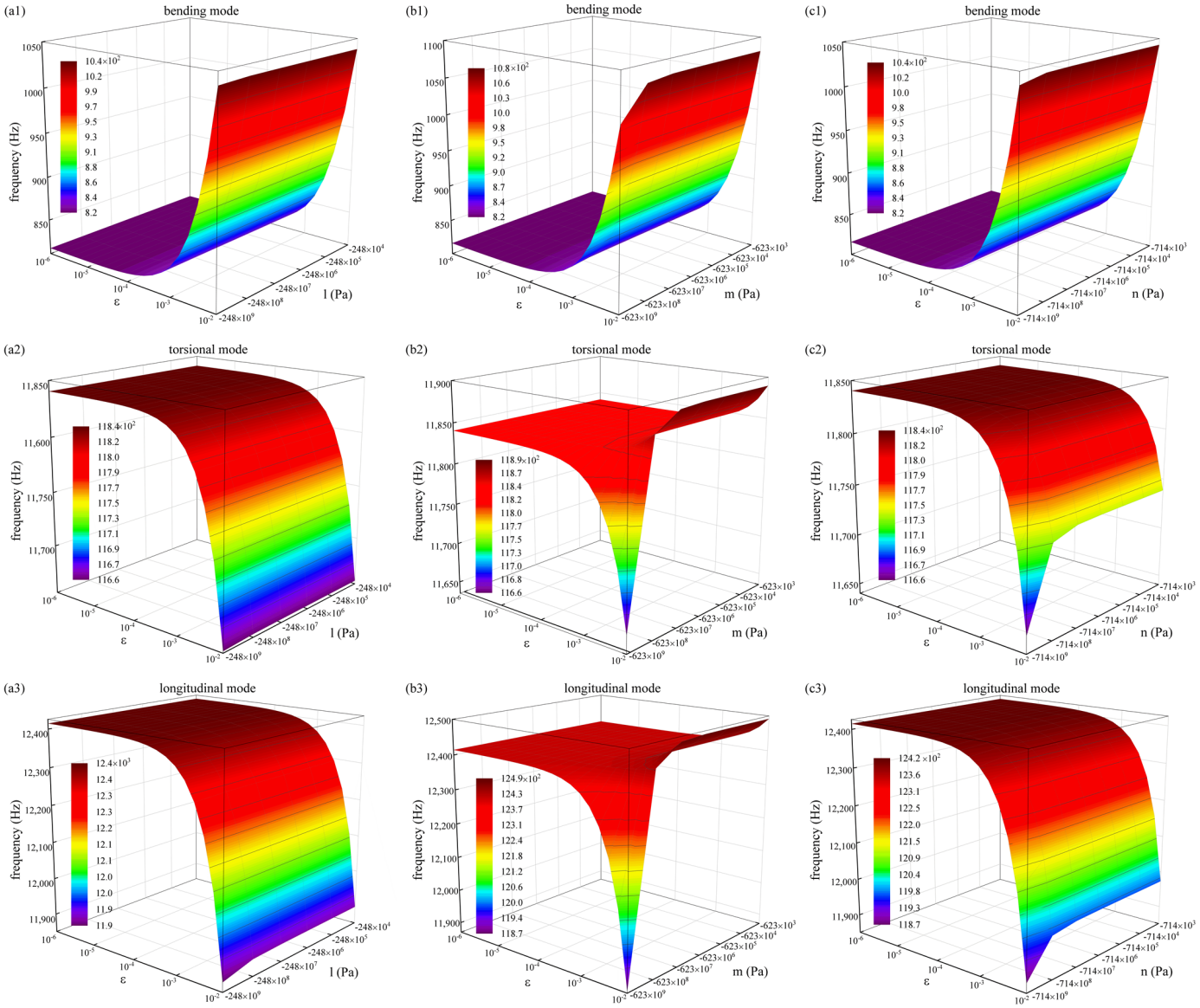

Figure 7. Surface diagram of mode frequency under strain and Murnaghan's third-order elastic constant change. (**a1**) surface diagram of bending mode frequency under strain and l change; (**a2**) surface diagram of torsional mode frequency under strain and l change; (**a3**) surface diagram of longitudinal mode frequency under strain and l change; (**b1**) surface diagram of bending mode frequency under strain and m change; (**b2**) surface diagram of torsional mode frequency under strain and m change; (**b3**) surface diagram of longitudinal mode frequency under strain and m change; (**c1**) surface diagram of bending mode frequency under strain and n change; (**c2**) surface diagram of torsional mode frequency under strain and n change; (**c3**) surface diagram of longitudinal mode frequency under strain and n change.

Figure 7c illustrates that the frequency of the bolted structure changes in response to alterations in both the strain and Murnaghan's third-order elastic constant n. With regard to the bending mode (Figure 7(c1)), an increase in strain is accompanied by an increase in frequency, while there is only a slight change in frequency with an increase in n, with the exception of a slight decrease in frequency when the strain is 10^{-2} and n is -714×10^{9}Pa. In the torsional mode (Figure 7(c2)) and the longitudinal mode (Figure 7(c3)), the frequency demonstrates a decrease with the increase in strain and exhibits minimal variation with the increase in n. A notable decline in frequency is observed only when the strain is 10^{-2} and the Murnaghan's third-order elastic constant n is equal to -714×10^{9} Pa.

3.2.2. Influence of Bolted Structure Parameters on Natural Frequency Characteristics

This section examines the impact of bolt preload variation on the natural frequency of the structure for different bolt lengths and diameters. To this end, bolts with diameters of 30 mm and lengths of 160, 180, 200, 220, 240, and 260 mm were selected for analysis at the frequencies of the bending mode, torsional mode, and longitudinal mode under varying tensile strains. The findings are presented in Table 3.

Table 3. Mode fundamental frequency (Hz) with different bolt lengths under different strains.

Modes	Bolt Length (mm)	Strain ε					
		0	$\mathbf{10^{-6}}$	$\mathbf{10^{-5}}$	$\mathbf{10^{-4}}$	$\mathbf{10^{-3}}$	$\mathbf{10^{-2}}$
bending mode	160	1251.1052	1251.1310	1251.3626	1253.6743	1276.3310	1462.4871
	180	999.6774	999.7043	999.9459	1002.3572	1025.9347	1217.7101
	200	816.4894	816.5171	816.7656	819.2445	843.4099	1036.5595
	220	679.0554	679.0836	679.3371	681.8648	706.4184	898.8077
	240	573.2732	573.3018	573.5590	576.1223	600.9244	791.1777
	260	490.3680	490.3969	490.6568	493.2466	518.1976	705.3551
torsional mode	160	14,758.2860	14,758.2647	14,758.0733	14,756.1568	14,736.7916	14,521.3192
	180	13,139.7706	13,139.7520	13,139.5841	13,137.9032	13,120.9241	12,932.7591
	200	11,840.5873	11,840.5707	11,840.4212	11,838.9246	11,823.8100	11,656.6958
	220	10,774.1496	10,774.1346	10,773.9998	10,772.6499	10,759.0183	10,608.4617
	240	9883.7275	9883.7139	9883.5914	9882.3652	9869.9843	9733.5249
	260	9129.2540	9129.2415	9129.1291	9128.0043	9116.6478	8991.5975
longitudinal mode	160	15,366.3660	15,366.3057	15,365.7626	15,360.3260	15,305.3337	14,680.9919
	180	13,737.3769	13,737.3234	13,736.8418	13,732.0213	13,683.2901	13,134.8923
	200	12,414.3921	12,414.3440	12,413.9115	12,409.5820	12,365.8280	11,875.3106
	220	11,322.5266	11,322.4830	11,322.0902	11,318.1582	11,278.4294	10,833.7621
	240	10,405.5042	10,405.4644	10,405.1054	10,401.5126	10,365.2200	9960.6934
	260	9625.6932	9625.6564	9625.3258	9622.0160	9588.5866	9216.4303

Figure 8 reflects the influence of bolt length and strain change on the fundamental frequency of the mode from three aspects. Among them, Figure 8a shows the changing trend in the fundamental frequency of the bolted structure affected by strain and bolt length in the 3D diagram as a whole. In Figure 8b, the variation curves of different mode frequencies of the bolted structure under tensile strain are depicted. Additionally, Figure 8c demonstrates the change in bolted structure frequency with varying bolt length, with the gray shaded area representing a frequency range of 10^{-2} and no strain. Let $\Delta\varepsilon = |\varepsilon_{0.01} - \varepsilon_0|$, which denotes the absolute value of the frequency difference between 10^{-2} strain and zero strain (shown as a rose-red dot line). It is more sensible to observe that the frequency trend changes with varying bolt lengths when comparing strained and no-strain conditions.

The bending mode frequency of the bolt rises as the bolt tensile strain increases, as seen in Figure 8(b1). When exposed to varying stresses, bolts of various lengths generally exhibit a similar changing trend. In the initial deformation stage, where the strain value is less than 10^{-4}, there is hardly any change in mode frequency. However, when the strain value exceeds 10^{-4}, the mode frequency begins to rise nonlinearly with increasing strain. Figure 8(c1) demonstrates that the bending mode frequency decreases with an increase in bolt length, where $\Delta\varepsilon$ first rises and then decreases with increasing bolt length.

As illustrated in Figure 8(b2), the torsional mode frequency of a bolt decreases slightly as it is subjected to tensile strain. This decrease is observed with an increase in bolt strain, and the overall change trend of bolts of different lengths remains similar when subjected to different strains. Specifically, in the initial stage of small deformation where the strain value is less than 10^{-3}, there is hardly any change in mode frequency. However, once the strain value exceeds 10^{-3}, the mode frequency begins to change, showing a nonlinear decrease with increasing strain. Figure 8(c2) demonstrates that as the length of the bolt increases, its torsional mode frequency decreases while $\Delta\varepsilon$ also decreases accordingly.

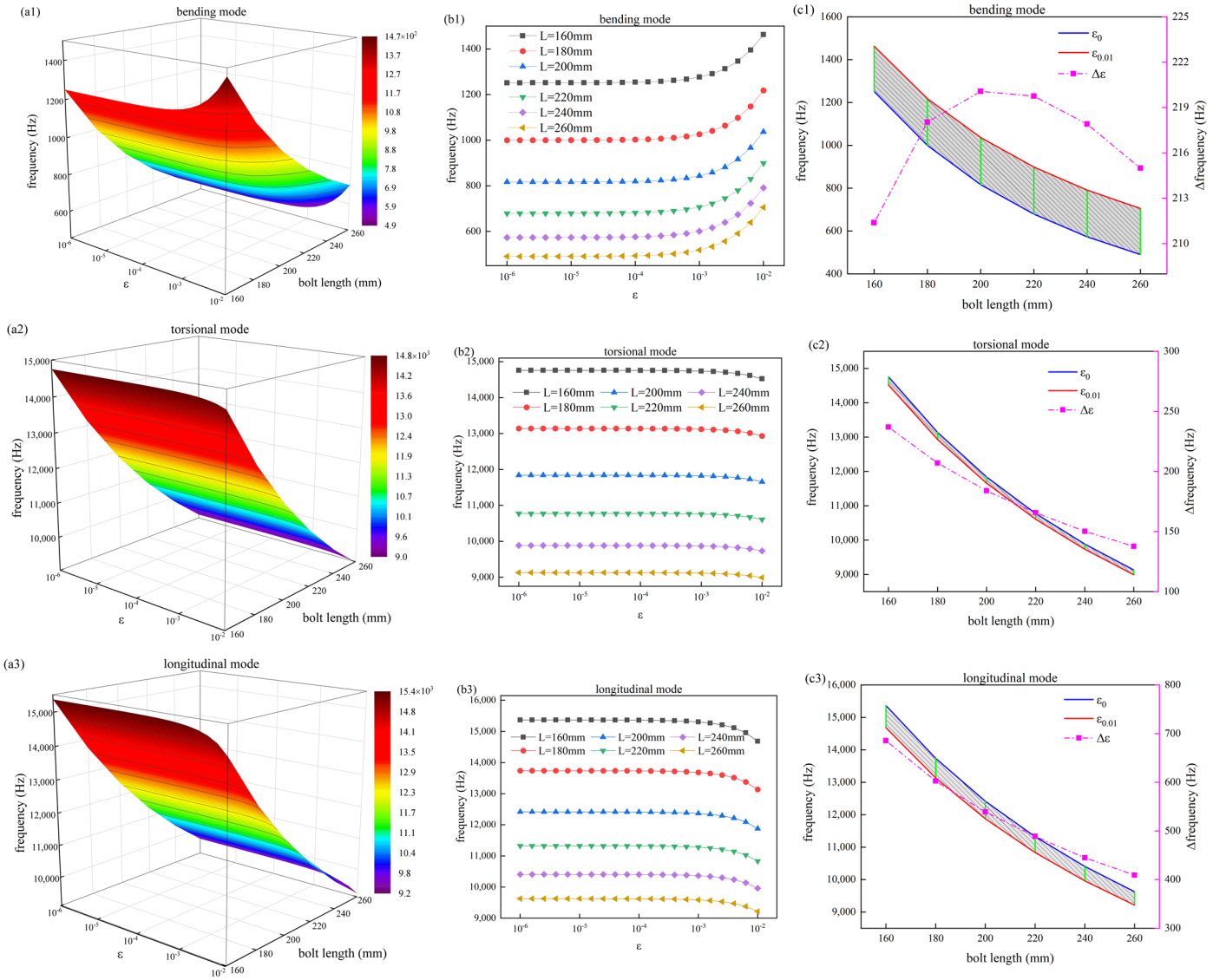

Figure 8. Influence of bolt length and strain changes on fundamental frequency. (**a1**) surface diagram of bending mode frequency under strain and bolt length change; (**a2**) surface diagram of torsional mode frequency under strain and bolt length change; (**a3**) surface diagram of longitudinal mode frequency under strain and bolt length change; (**b1**) curve graph of bending mode frequency under strain and bolt length change; (**b2**) curve graph of torsional mode frequency under strain and bolt length change; (**b3**) curve graph of longitudinal mode frequency under strain and bolt length change; (**c1**) differential chart of bending mode frequency under no strain and 0.01 strain; (**c2**) differential chart of torsional mode frequency under no strain and 0.01 strain; (**c3**) differential chart of longitudinal mode frequency under no strain and 0.01 strain.

As shown in Figure 8(b3), the longitudinal mode frequency of a bolt under tensile strain decreases with the increase in bolt strain. When subjected to different strains, the overall change trend of bolts of various lengths is similar. In the small deformation stage, the strain value is less than 10^{-3}, and the mode frequency hardly changes. When the strain value exceeds 10^{-3}, the mode frequency begins to change, and the longitudinal mode frequency decreases nonlinearly with the increase in the strain. When the bolt length changes, its frequency decreases with the increase in bolt length, and its difference decreases with the increase in bolt length. Figure 8(c3) shows that the longitudinal mode frequency decreases as the bolt length increases, and $\Delta\varepsilon$ decreases as the bolt length increases.

To investigate the influence of bolt diameter on natural frequency, bolts ranging from 20, 24, 30, 36, 42, 48, and 56 mm in diameter were studied separately. A length of 200 mm was chosen in accordance with the standards, and the results are shown in Table 4.

Table 4. Mode fundamental frequency (Hz) with different bolt diameters under different strains.

Modes	Bolt Diameter (mm)	Strain ε					
		0	10^{-6}	10^{-5}	10^{-4}	10^{-3}	10^{-2}
bending mode	m20	556.0075	556.0515	556.4473	560.3864	597.9781	867.2763
	m24	661.7927	661.8287	662.1521	665.3746	696.4897	932.5279
	m30	816.4706	816.4982	816.7468	819.2257	843.3908	1036.5284
	m36	964.8648	964.8866	965.0829	967.0414	986.2233	1143.3586
	m42	1106.5374	1106.5548	1106.7115	1108.2758	1123.6285	1250.2272
	m48	1241.7633	1241.7773	1241.9032	1243.1599	1255.4958	1355.3737
	m56	1409.4438	1409.4542	1409.5472	1410.4757	1419.5657	1488.2257
torsional mode	m20	11,881.8176	11,881.8016	11,881.6569	11,880.2087	11,865.5911	11,705.0988
	m24	11,864.9056	11,864.8893	11,864.7427	11,863.2756	11,848.4636	11,685.3448
	m30	11,840.5147	11,840.4981	11,840.3486	11,838.8522	11,823.7392	11,656.6415
	m36	11,815.2532	11,815.2363	11,815.0838	11,813.5572	11,798.1335	11,626.7273
	m42	11,786.5573	11,786.5401	11,786.3852	11,784.8344	11,769.1594	11,594.1859
	m48	11,758.2861	11,758.2686	11,758.1104	11,756.5275	11,740.5192	11,560.4818
	m56	11,717.8232	11,717.8052	11,717.6434	11,716.0230	11,699.6249	11,513.2325
longitudinal mode	m20	12,560.5105	12,560.4628	12,560.0340	12,555.7417	12,512.4062	12,032.7104
	m24	12,501.1768	12,501.1290	12,500.6986	12,496.3903	12,452.8744	11,968.4747
	m30	12,414.3149	12,414.2668	12,413.8343	12,409.5048	12,365.7510	11,875.2266
	m36	12,321.2757	12,321.2275	12,320.7931	12,316.4446	12,272.4644	11,773.9822
	m42	12,216.9599	12,216.9117	12,216.4777	12,212.1327	12,168.1574	11,665.5454
	m48	12,115.4487	12,115.4007	12,114.9690	12,110.6510	12,065.6764	11,553.3148
	m56	11,959.0018	11,958.9538	11,958.5215	11,954.1922	11,910.2540	11,384.7374

Figure 9 reflects the influence of bolt diameter and strain change on the fundamental frequency of the mode from three aspects. Among them, Figure 9a shows the changing trend of the fundamental frequency of the bolted structure affected by strain and bolt diameter in the 3D diagram as a whole. In Figure 9b, the curves depict the variation in different mode frequencies of the bolted structure under tensile strain. Additionally, Figure 9c) displays how the bolted structure's frequency varies with bolt diameter changes. The shaded gray area represents the frequency range between a strain of 10^{-2} and no strain, while the dotted line indicates the absolute value $\Delta\varepsilon = |\varepsilon_{0.01} - \varepsilon_0|$ of the frequency difference between a strain of 10^{-2} and zero strain.

As shown in Figure 9(b1), the bending mode frequency of a bolt increases with an increase in tensile strain. The overall change trend for bolts of different lengths is similar when subjected to different strains. In the initial stage of small deformation, where the strain value is less than 10^{-4}, there is hardly any change in mode frequency. However, when the strain value exceeds 10^{-4}, the mode frequency begins to change, and it rises nonlinearly with an increase in strain. Figure 9(c1) demonstrates that the bending mode frequency increases with an increase in the bolt diameter, while $\Delta\varepsilon$ decreases as the bolt length increases, and this reduction is significant.

As illustrated in Figure 9(b2), the torsional mode frequency of a bolt decreases as it is subjected to tensile strain. This decrease in frequency is observed with an increase in bolt strain, and the overall trend remains similar for bolts of different lengths when subjected to varying strains. In the initial stage of small deformation, where the strain value is less than 10^{-4}, there is minimal change in the mode frequency. However, once the strain value exceeds 10^{-4}, the mode frequency begins to change nonlinearly, decreasing with an increase in strain. Figure 9(c2) demonstrates that as the bolt diameter increases, so does the decrease in torsional mode frequency, while $\Delta\varepsilon$ also increases with an increase in bolt length.

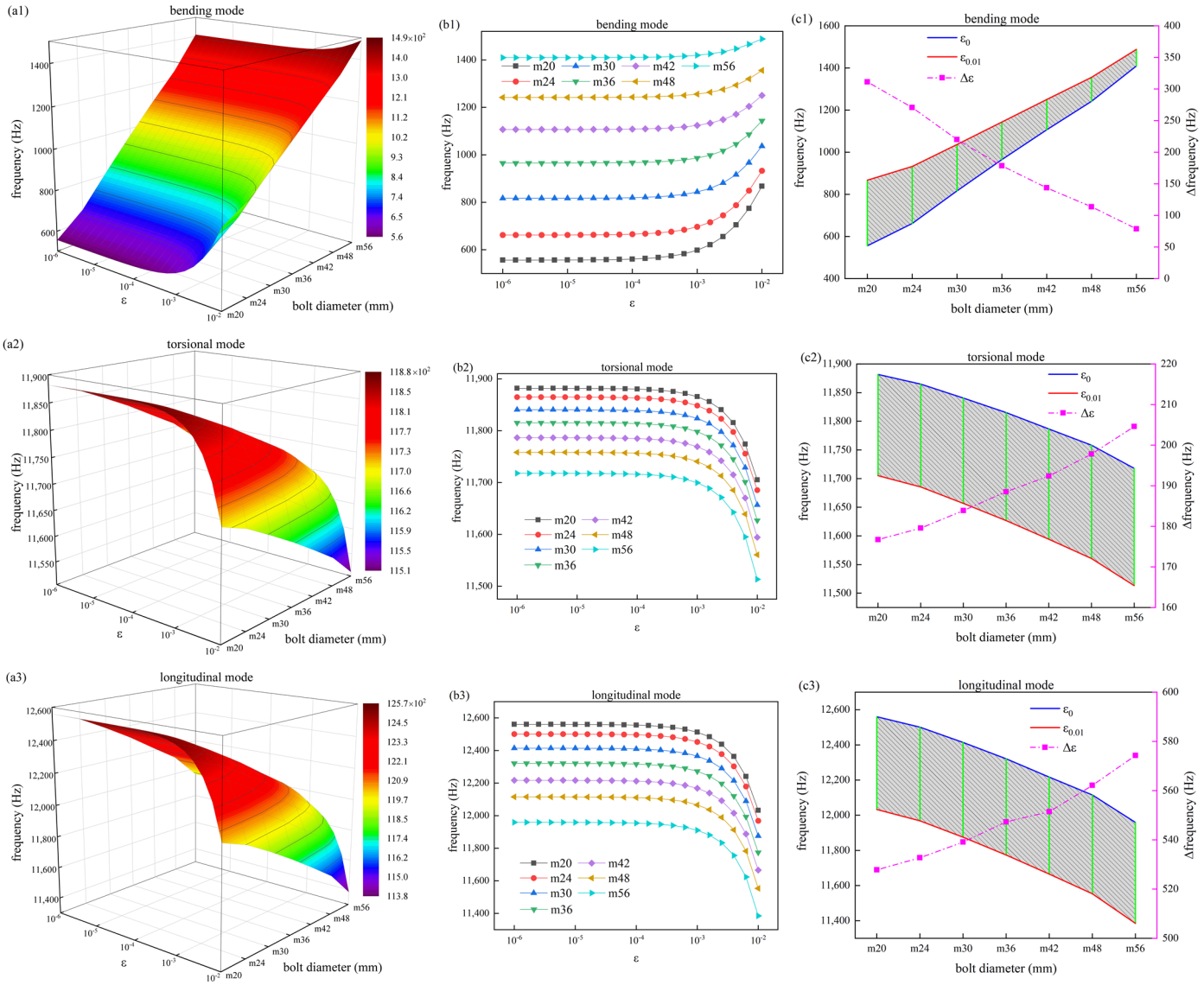

Figure 9. Influence of bolt diameter and strain changes on fundamental frequency. (**a1**) surface diagram of bending mode frequency under strain and bolt diameter change; (**a2**) surface diagram of torsional mode frequency under strain and bolt diameter change; (**a3**) surface diagram of longitudinal mode frequency under strain and bolt diameter change; (**b1**) curve graph of bending mode frequency under strain and bolt diameter change; (**b2**) curve graph of torsional mode frequency under strain and bolt diameter change; (**b3**) curve graph of longitudinal mode frequency under strain and bolt diameter change; (**c1**) differential chart of bending mode frequency under no strain and 0.01 strain; (**c2**) differential chart of torsional mode frequency under no strain and 0.01 strain; (**c3**) differential chart of longitudinal mode frequency under no strain and 0.01 strain.

As depicted in Figure 9(b3), the longitudinal mode frequency of a bolt decreases as it is subjected to tensile strain. This decrease in frequency is observed with an increase in bolt strain, and the overall trend remains similar for bolts of different lengths when subjected to varying strains. In the initial stage of small deformation, where the strain value is less than 10^{-4}, there is minimal change in the mode frequency. However, as the strain value exceeds 10^{-4}, the mode frequency begins to exhibit a non-linear decrease with increasing strain. Figure 9(c3) further demonstrates that as the bolt diameter increases, so does the decrease in longitudinal mode frequency, while $\Delta\varepsilon$ increases with an increase in bolt length.

4. Conclusions

The objective of this study is to analyze the intrinsic properties of bolted structures with various preloads in order to investigate the fundamental frequency of different modes within a specified frequency range. This enables the accurate prediction of the acoustoelastic behavior of the structure in response to a range of conditions. Consequently, an investigation into the intrinsic characteristics of bolted structures represents a pivotal approach to both their design and the diagnosis of failure in engineering applications. The study of the acoustic elastic relationship of the structure is innovatively transformed into the study of the inherent characteristics of the structure. Through K' of Equation (22), the relationship between f_σ and f with ε is transferred, and the relationship between structure natural frequency and bolt prestress is further revealed. In this study, the main structural modes of bolts under different preloading forces were investigated, and the effects of the material parameters, Lame elastic constant, Murnaghan third-order elastic constant and bolt size parameters were investigated. The results show that the natural frequencies of different vibration modes can be used to predict and detect the change in the preload of bolt structures. The analysis demonstrates that:

(i) The study of bolts made of various materials shows that the general change trend is the same, and the natural frequency under different structural modes has an obvious change trend under different preloading forces. Specifically, the bending mode frequency demonstrates an augmentation with increasing preload, whereas the torsional and longitudinal mode frequencies display a reduction.

(ii) The parameters of high manganese steel were chosen as the base research parameters to investigate the variation in bolt natural frequency with preloads when altering the Lame elastic constants λ, μ in this study. For λ, the bending mode frequency increases with an increase in preload. While the torsional and longitudinal modes decrease when λ changes in a small range, as λ reaches a large value, the effect of preload on frequency becomes less pronounced. In contrast, there is no significant overall change in the frequencies of the three modes with increasing preload for μ.

(iii) The parametric studies of Murnaghan's third-order elastic constants l, m, n, show that the change in the elastic constants is weaker than the pattern of change in the fundamental frequency of the structure embodied in the preload force, and the frequency of l in bending mode increases with preload, while the frequency of l in torsional and longitudinal modes decreases with preload. As for m, the frequency in the bending mode increases with preload, while the frequencies in the torsional and longitudinal modes mainly increase with preload. However, when m $= -623\times10^9$ Pa, the frequency decreases with increasing preload. In the case of n, the bending mode frequency increases with preload, whereas the frequencies in the torsional and longitudinal modes decrease with increasing preload.

(iv) The structure parameters of bolts are studied in this paper. It is observed that the bending mode frequency increases with an increase in preload, while the torsional mode frequency and longitudinal mode frequency decrease with an increase in preload. In the bending mode, the frequency value of $\Delta\varepsilon$ initially increases and then decreases with an increase in bolt length. It decreases with an increase in bolt diameter. In the torsion mode and longitudinal mode, the frequency value of $\Delta\varepsilon$ decreases with an increase in bolt length and increases with an increase in bolt diameter.

In future research, we will analyze and consider the effect of various complex external conditions on the intrinsic properties of the equipment structure in the presence of preload. These conditions include wind load, temperature difference, and extreme conditions such as high salt and high humidity environments. The goal is to more realistically simulate the working conditions of the components in actual applications. The utilization of finite element analysis software and supercomputing platforms for the study of large structural components enables the accurate simulation and restoration of actual working conditions, thereby ensuring that the simulation results are more closely aligned with the real situation.

This is not only conducive to more effective use of theoretical analysis and simulation analysis to comprehensively verify the preload force on the structural intrinsic properties of the law, but also markedly enhances the precision of data and the depth of analysis. The application of online monitoring technology for structural intrinsic properties realizes the real-time monitoring of in-service bolts, thus ensuring the safety and stability of bolts in key technological fields such as aviation and marine. The integration of these studies and technologies will facilitate the development of a more precise and efficient solution for the maintenance and inspection of bolts, thereby advancing the technological advancement of related fields while enhancing the durability and reliability of equipment. On this basis, in conjunction with the subsequent experimental analysis, the reliability of bolt preload detection can be significantly enhanced, thereby providing a more robust assurance for the design and practical implementation of large structural components. This approach effectively integrates theoretical, simulation, and experimental methodologies, thereby further enhancing the scientific rigor of the analysis and the reliability of the results.

Author Contributions: Conceptualization, L.Z. and R.K.; methodology, L.Z.; software, R.K.; validation, G.T., X.S. and L.S.; formal analysis, L.Z.; investigation, X.S.; resources, L.S.; data curation, R.K.; writing—original draft preparation, R.K.; writing—review and editing, L.Z.; visualization, R.K.; supervision, G.T.; project administration, X.S.; funding acquisition, L.Z. All authors have read and agreed to the published version of the manuscript.

Funding: This research was funded by the general project of natural science research of Institutions of Higher Education of Jiangsu Province of China, grant number No. 21KJB510016 and National Natural Science Foundation of China, grant number No. 62203193.

Data Availability Statement: The original contributions presented in the study are included in the article; further inquiries can be directed to the corresponding author.

Conflicts of Interest: The authors declare that the research was conducted in the absence of any commercial or financial relationships that could be construed as potential conflicts of interest.

References

1. Liu, H.B.; Zhang, X.; Liu, Y.K.; Wang, Y.Q. Research on electromagnetic ultrasonic unidirectional stress transverse and longitudinal wave joint measurement method. *Mech. Des. Manuf.* **2021**, *9*, 241–246. [CrossRef]
2. Zhang, X. EMAT-Based Unidirectional Stress Transverse and Longitudinal Wave Joint Measurement Method. Master's Thesis, Dalian University of Technology, Dalian, China, 2019. [CrossRef]
3. Lian, J.; Qian, Y.; Dong, L. Research on the effect of assembly process on the preload force of ultra-high-speed test shaft system. *Aerosp. Manuf. Technol.* **2018**, *2*, 52–56.
4. Xin, J. Ultrasonic Non-Destructive Testing and Calibration Technique for Gear Tooth Root Residual Stress. Master's Thesis, Beijing University of Technology, Beijing, China, 2015.
5. Lv, Y.; Zhang, X.; Gao, J.; Song, G.; He, C. Method and system for axial stress detection of bolts based on acoustoelastic effect. *Nondestruct. Test.* **2023**, *45*, 11–15.
6. Lv, Y.; Xie, L.; Song, G.; He, C.; Cheng, J.; Ji, S. A method for axial stress detection of bolts based on acoustoelastic effect. *J. Beijing Inst. Technol.* **2022**, *48*, 920–927.
7. Gao, S. Research on Electromagnetic Ultrasonic Detection of Wind Turbine Bolt Stress. Master's Thesis, Shenyang University of Technology, Shenyang, China, 2022. [CrossRef]
8. Lee, S.-H. Research on the Measurement Technique of High Tensile Bolt Pre-Tension by Ultrasonic Double Wave Method. Master's Thesis, Beijing University of Architecture, Beijing, China, 2023. [CrossRef]
9. Pan, Q.; Chang, M.; Pan, R.; Xu, X.; Li, S.; Zhang, Y. Research on nonlinear ultrasonic detection technology of bolt axial stress. *J. Mech. Eng.* **2021**, *57*, 88–95.
10. Feng, S. Research on Ultrasonic Detection Method of Axial Stress in High Strength Bolts. Master's Thesis, Hubei University of Technology, Wuhan, China, 2022. [CrossRef]
11. Feng, S.; Tu, J.; Wei, S.; Chi, Y.; Zhang, X.; Song, X. Ultrasonic testing of axial stress of high strength bolts for bridges. *Int. J. Appl. Electromagn. Mech.* **2020**, *64*, 685–692. [CrossRef]
12. Crecraft, D.I. Ultrasonic measurement of stresses. *Ultrasonics* **1968**, *6*, 117–121. [CrossRef]
13. Kwaśniewki, J. Influence of acoustoelastic coefficient on wave time of flight in stress measurement in piezoelectric self-excited system. *Mech. Syst. Signal Process.* **2016**, *78*, 143–155. [CrossRef]
14. Zhao, X.-X.; Li, Y.-M.; Liu, X.-G.; Yao, K. Ultrasonic measurement on axial force of high-strength bolt in service. *J. Low Freq. Noise Vib. Act. Control.* **2020**, *39*, 596–603. [CrossRef]

15. Kelardeh, S.M.; Hosseini, S.V.; Heidari, M.; Parvaz, H. An investigation of the effect of bolt tightening stress on ultrasonic velocity in cylinder head and main bearing cap bolts of diesel engine. *J. Braz. Soc. Mech. Sci. Eng.* **2021**, *43*, 375. [CrossRef]
16. Mills, B.; Javadi, Y.; Abad, F.; Lotfian, S.; MacLeod, C.; Mehmanparast, A.; Pierce, G.; Gachagan, A. Inspection of wind turbine bolted connections using the ultrasonic phased array system. *Heliyon* **2024**, *10*, e34579. [CrossRef]
17. Leng, J.; Tian, H.; Zhou, G.; Wu, Z. A review of research on dynamic damage diagnosis methods for in-service offshore platforms. *Chin. J. Saf. Sci.* **2017**, *27*, 79–85. [CrossRef]
18. Zhao, G.; Jin, X.; Cui, Y.; Feng, Z.; Wang, T.; Xiong, Z. A contact stiffness identification method based on modal strain energy. *J. Mech. Eng.* **2020**, *56*, 147–153.
19. Gou, B.; Lu, Q.; Wang, B.; Wang, S. Detection of bolt tightening force using intrinsic frequency outlier analysis. *Vib. Shock* **2015**, *34*, 77–82.
20. An, W.W.; Guo, B.; Gong, Z.R. A dynamic stiffness identification method for bolted joints based on modal experiments. *Mech. Des. Manuf.* **2015**, *2*, 1–3+7.
21. Zhao, G.; Wang, B.; Yu, G.; Yang, H.; Huang, X. Study on the influence law of bolt preload on the characteristic parameters of bolt bonding surface. *Mech. Strength* **2018**, *40*, 392–397. [CrossRef]
22. Zhao, G.; Xiong, Z.; Jin, X.; Hou, L.; Gao, W. Prediction of contact stiffness in bolted interface with natural frequency experiment and FE analysis. *Tribol. Int.* **2018**, *127*, 157–164. [CrossRef]
23. Sah, S.M. Estimating bolt tightness using transverse natural frequencies. *J. Sound Vib.* **2018**, *431*, 137–149. [CrossRef]
24. Bonisoli, E.; Marcuccio, G. Venturini, Interference fit estimation through stress-stiffening effect on dynamics. *Mech. Syst. Signal Process.* **2021**, *160*, 107919. [CrossRef]
25. de Faria, A.R.; Donadon, M.V. The use of piezoelectric stress stiffening to enhance buckling of laminated plates. *Lat. Am. J. Solids Struct.* **2009**, *7*, 167–183. [CrossRef]
26. Han, X. Study on the Dynamic Characteristics of Bolted Flange Connection Structures Considering the Connection State. Master's Thesis, Xi'an University of Science and Technology, Xi'an, China, 2021. [CrossRef]
27. Michael, W. Bolted Joint Preload Distribution from Torque Tightening. *Stroj. Časopis-J. Mech. Eng.* **2021**, *71*, 329–342. [CrossRef]
28. Egle, D.M.; Bray, D.E. Measurement of acoustoelastic and third-order elastic constants for rail steel. *J. Acoust. Soc. Am.* **1976**, *60*, 741–744. [CrossRef]